ResearchGate

See discussions, stats, and author profiles for this publication at: https://www.researchgate.net/publication/6793317

Trifluoroethanol-Induced β → α Transition in β-Lactoglobulin: Hydration and Cosolvent Binding Studied by 2H, 17O, and 19F Magnetic Relaxation Dispersion

ARTICLE *in* BIOCHEMISTRY · DECEMBER 2003

Impact Factor: 3.02 · DOI: 10.1021/bi035330l · Source: PubMed

CITATIONS
28

READS
18

3 AUTHORS, INCLUDING:

Sandeep Kumar
Rajiv Gandhi University of Health Sciences, K…
5 PUBLICATIONS **89** CITATIONS
SEE PROFILE

Kristofer Modig
Lund University
16 PUBLICATIONS **623** CITATIONS
SEE PROFILE

Available from: Kristofer Modig
Retrieved on: 01 February 2016

Trifluoroethanol-Induced $\beta \rightarrow \alpha$ Transition in β-Lactoglobulin: Hydration and Cosolvent Binding Studied by ^{2}H, ^{17}O, and ^{19}F Magnetic Relaxation Dispersion†

Sandeep Kumar,‡ Kristofer Modig, and Bertil Halle*

Department of Biophysical Chemistry, Lund University, SE-22100 Lund, Sweden

Received July 25, 2003; Revised Manuscript Received September 19, 2003

ABSTRACT: Alcohols, such as 2,2,2-trifluoroethanol (TFE), have been shown to induce a cooperative transition to an open helical structure in many proteins, but the underlying molecular mechanism has not been identified. Here, we employ the technique of magnetic relaxation dispersion (MRD) to study the TFE-induced $\beta \rightarrow \alpha$ transition of β-lactoglobulin at pH 2.4. Unlike traditional techniques that focus on protein secondary structure, the MRD method directly monitors the solvent, providing quantitative information about preferential solvation and solvent penetration and about the overall size and structural integrity of the protein. In this multinuclear MRD study, we use the ^{2}H and ^{17}O resonances to examine hydration and the ^{19}F resonance to study TFE. The transformation from the native to the helical state via an intermediate state at 300 K is found to be accompanied by a progressive expansion of the protein and loss of specific long-lived hydration sites. The observation of ^{17}O and ^{19}F dispersions from the helical state shows that water and TFE penetrate the protein. The MRD data indicate a strong accumulation of TFE at the surface as well as in the interior of the protein. At 277 K, BLG is much less affected by TFE, remaining in the native state at 16% TFE, but adopting a nonnative structure at 30% TFE. This nonnative structure is not penetrated by long-lived water molecules. The implications of these findings for the mechanism of TFE-induced structural transformations are discussed.

Fluorinated alcohols, such as 2,2,2-trifluoroethanol (TFE),[1] have long been known to stabilize regular secondary structure, in particular α-helices, in peptides (*1*−*12*). More recently, it has been shown that TFE can trigger a cooperative transition to an open helical structure in many proteins (*13*−*16*). Apparently, TFE allows amino acid residues to manifest their intrinsic helical propensity, which may be suppressed by nonlocal interactions in the native protein (*2*, *14*, *17*).

Bovine β-lactoglobulin (BLG), the major whey protein in cow's milk, has been widely used as a model for studies of the alcohol-induced $\beta \rightarrow \alpha$ transition in proteins (*13*, *17*−*29*). A member of the lipocalin superfamily, native BLG consists of nine antiparallel strands in a β-barrel fold enclosing a large cavity that binds retinol, fatty acids, and other nonpolar molecules (*30*−*33*). BLG forms a dimer under physiological conditions, but is monomeric at pH 2−3 in the absence of salt (*34*). The 48% α-helix content predicted theoretically greatly exceeds the level of 7% found in the crystal structure of BLG (*13*), consistent with the finding that isolated BLG fragments may adopt nonnative helical structure in aqueous solution and invariably do so in the presence of TFE (*3*, *35*). BLG undergoes a $\beta \rightarrow \alpha$ transition in the range of 15−20% TFE, with the helix content increasing from 7% in the native protein (N) to 60−80% in the helical state (H) at 30% TFE (*13*, *17*−*29*). Several studies indicate that the TFE-induced structural transformation is best described as a three-state equilibrium, N ↔ I ↔ H, with the intermediate state (I) being most populated around 15−20% TFE (*23*, *26*).

Although the effects of TFE on peptides and proteins have been thoroughly studied, no consensus has emerged about the underlying molecular mechanisms. Most studies have focused on peptides (*1*−*12*), where the relevant equilibrium involves unstructured and helical forms (U ↔ H). One may then ask whether TFE shifts the equilibrium by stabilizing the H form, destabilizing the U form, or both. It is frequently assumed that the peptide is preferentially solvated by TFE, i.e., that TFE accumulates near the peptide−solvent interface. Direct evidence for such preferential solvation has recently come from intermolecular NOE measurements (*36*−*38*) and molecular simulations (*37*−*40*). Whether the principal effect of TFE is to strengthen intrapeptide hydrogen bonds (because TFE is a less polar solvent than water and a less potent hydrogen bond competitor) or to weaken hydrophobic interactions among side chains (by displacing water and modifying its structure) is less clear.

Because the TFE-induced N ↔ H equilibrium in proteins does not involve the unfolded state, the thermodynamics and mechanism may differ considerably from the peptide case. While CD and high-resolution NMR studies have elucidated the dependence of protein secondary structure on TFE concentration, little direct information about the critical role of protein solvation in TFE/water mixtures is available.

† This work was supported by the Crafoord Foundation and the Swedish Research Council.

* To whom correspondence should be addressed. Phone: +46-46-222 9516. Fax: +46-46-222 4543. E-mail: bertil.halle@bpc.lu.se.

‡ Present address: Department of Chemistry, The Ohio State University, Columbus, OH 43210.

[1] Abbreviations: BLG, β-lactoglobulin; CD, circular dichroism; MRD, magnetic relaxation dispersion; NMR, nuclear magnetic resonance; NOE, nuclear Overhauser effect; SDF, spectral density function; TFE, trifluoroethanol.

10.1021/bi035330l CCC: $25.00 © 2003 American Chemical Society
Published on Web 10/30/2003

Molecular dynamics simulations on the time scale of the N → H transition are not yet feasible, and the only reported intermolecular NOE study (on hen egg white lysozyme at pH 2) detected TFE binding in the active site but did not provide quantitative results on preferential solvation or solvent penetration (*41*).

Here, we use the technique of magnetic relaxation dispersion (MRD) to monitor directly the interactions of water and TFE with BLG in native and TFE-induced nonnative states. The MRD method has been used extensively to study the hydration of native proteins and nucleic acids (*42*−*45*) and has also been applied to proteins denatured by heat (*46*), guanidinium chloride (*47*), or urea (*68*), to proteins in the molten-globule state (*47*), and to proteins in a mixed DMSO/water solvent (*48*). By measuring the spin relaxation rates of solvent species over a wide range of resonance frequencies, one obtains a spectral density function that contains information about the number of solvent molecules interacting with the protein and about the time scale of these interactions (*44*, *45*). In the study presented here, we use the ^{2}H and ^{17}O resonances to monitor hydration and the ^{19}F resonance to examine TFE−protein interactions. While ^{19}F MRD has been used in solids (*49*), this appears to be the first biomolecular application.

MATERIALS AND METHODS

Sample Preparation. β-Lactoglobulin isoform A, prepared from the milk of homozygous cows at the INRA Laboratoire de Recherche de Technologie Laitière (Paris, France), was generously supplied by C. Holt of the Hannah Research Institute (Ayr, Scotland). The preparation used for measurements at 27 °C was first purified by anion exchange chromatography (DEAE-sephacel) at pH 6.0 (10 mM MES buffer) and eluted with a 25 to 300 mM NaCl gradient. It was further purified by size-exclusion chromatography (Sephadex G-50) at pH 2.7 (10 mM citric acid and 50 mM NaCl). The protein was then dialyzed against milli-Q water and lyophilized. A second preparation, used for the 4 °C measurements, was prepared without the anion exchange step and with a Sephadex G-75 gel filtration column. Gel filtration removes a high-molecular weight impurity that amounts to ca. 1% of the protein (*69*). The two preparations produced identical MRD profiles, and low-frequency (field-cycling) ^{1}H MRD measurements demonstrated that they were free from high-molecular weight impurities (*69*).

The NMR samples were prepared by dissolving the lyophilized protein in ^{2}H- and ^{17}O-enriched water (25 at. % ^{2}H and 9.5 at. % ^{17}O), prepared from pure H_2O with a low level of paramagnetic impurities (Fluka BioChemika), D_2O (99.9%, CIL), and $H_2{}^{17}O$ (19%, Isotec). For samples with TFE, the water contained 50 at. % ^{2}H, and TFE (>99.5%, Aldrich) was added to a final concentration of 16 or 30% (v/v). The pH was adjusted to 2.4 (uncorrected for isotope effects) in all samples by adding small amounts of HCl. A small fraction of insoluble protein was removed by centrifugation. The protein concentration, C_P, was determined by complete amino acid analysis of each sample. After completion of the ^{2}H and ^{17}O MRD experiments at 27 °C and before the ^{19}F measurements, argon gas was bubbled through the solutions for 2 h. This eliminates most of the dissolved O_2, a paramagnetic species which otherwise would make a significant contribution to the ^{19}F relaxation. Because argon bubbling also removes some of the volatile TFE, the TFE concentration in these samples was redetermined by HPLC (performed by Mikrokemi AB, Uppsala, Sweden) after the ^{19}F MRD measurements.

Table 1: Characteristics of MRD Samples

no.	T (°C)	TFE (vol %)	C_P (mM)	N_T^W ($\times 10^3$)	N_T^{TFE} ($\times 10^3$)	D_2O (at. %)	η^a (cP)	$\tau_R{}^b$ (ns)
1	4	0	0.53	103.6	0	25	1.69	19.6
2	4	16	0.57	81.9	3.90	50	3.24[d]	34.6
3	4	30	0.60	65.2	6.98	50	4.17	48.2
4	27	0	0.92	59.4	0	25	0.90	9.6
5	27	16	0.89	52.3	2.49	50	1.37	14.6
6	27	29	0.86	46.0	4.69	50	1.66	17.7
7[c]	27	7	0.99	51.6	0.97	50	1.14	12.1
8[c]	27	21	0.95	46.1	3.06	50	1.48	15.9

[a] The viscosity η of TFE/H_2O mixtures was obtained from refs *64* and *65*. The H/D isotope effect on η was assumed to be the same as in the absence of TFE. [b] Rotational correlation time of BLG in the native state, estimated by scaling the experimental value (*32*) according to $\tau_R \propto \eta/T$. [c] Samples 7 and 8 correspond to samples 5 and 6, respectively, after O_2 purging with argon. [d] Viscosity not found in the literature, assumed to scale with R_{bulk} (see Table 2).

For the analysis of the MRD data, we need the total water/protein (N_T^W) and TFE/protein (N_T^{TFE}) molar ratios. The water/TFE molar ratio can be obtained from the volume fraction of TFE (before mixing) and the molar volume of pure water and TFE. The N_T^W and N_T^{TFE} ratios can then be calculated from the protein concentration C_P, the density of the mixed solvent (*50*), and a small correction for the protein volume. Sample characteristics are collected in Table 1.

MRD Measurements. Magnetic relaxation dispersion profiles of the ^{2}H, ^{17}O, and ^{19}F longitudinal relaxation rate R_1 ($=1/T_1$) were acquired. Each dispersion profile is based on relaxation experiments at seven to nine magnetic field strengths, accessed with Varian 500 Unity Plus, Bruker Avance DMX 100, and DMX 200 NMR spectrometers and a field-variable iron-core magnet (Drusch EAR-35N) equipped with a field-variable lock and flux stabilizer and interfaced with a Tecmag Discovery console. The ^{17}O resonance frequency ranged from 2.2 to 67.8 MHz, the ^{2}H frequency from 2.5 to 76.7 MHz, and the ^{19}F frequency from 6.8 to 188.5 MHz. The sample temperature was adjusted with an accuracy of 0.1 °C by a thermostated air flow and was checked with a copper−constantan thermocouple referenced to an ice bath. As an additional temperature control, we measured the (field-independent) relaxation rates on protein-free reference samples with the same solvent composition as the protein solutions.

The relaxation time T_1 was measured by the inversion recovery method, using a 16-step phase cycle, 20 delay times in random order, and a sufficient number of transients to obtain a signal-to-noise ratio of at least 100 (*44*, *45*). T_1 was determined from a standard three-parameter fit. On the basis of the reproducibility of measurements on the reference samples, we estimate the accuracy in R_1 to ±0.5% for ^{2}H and ^{17}O and ±2% for ^{19}F (one standard deviation).

All MRD profiles were analyzed with an in-house Matlab implementation of the Levenberg−Marquardt nonlinear χ^2 minimization algorithm (*51*). To estimate the uncertainty in the fitted parameters, we performed fits on a Monte Carlo-generated ensemble of 1000 data sets, subject to random

Gaussian noise with a standard deviation of 0.5% for the ^{2}H and ^{17}O data and 2% for the ^{19}F data. Quoted uncertainties correspond to a confidence level of 68.3% (one standard deviation). The choice between single-Lorentzian and bi-Lorentzian spectral density functions (see below) was based on the *F* test with a cutoff probability of 0.9 (*51*, *52*).

Analysis of ^{2}H and ^{17}O MRD Data. The relaxation dispersion, $R_1(\omega_0)$, of the quadrupolar water nuclei ^{2}H and ^{17}O is given by (*44*, *45*)

$$R_1(\omega_0) = R_{bulk} + 0.2J(\omega_0) + 0.8J(2\omega_0) \quad (1)$$

where R_{bulk} is the frequency-independent relaxation rate of the bulk solvent, measured on a reference sample, and $J(\omega_0)$ is the frequency-dependent spectral density, with ω_0 ($=2\pi\nu_0$) being the ^{2}H or ^{17}O resonance frequency in angular frequency units. Most MRD profiles were modeled with a bi-Lorentzian spectral density function (SDF):

$$J(\omega) = \alpha + \frac{\beta\tau_\beta}{1 + (\omega\tau_\beta)^2} + \frac{\gamma\tau_\gamma}{1 + (\omega\tau_\gamma)^2} \quad (2)$$

The amplitude parameters α, β, and γ were converted to molecular parameters through (*44*, *45*)

$$\alpha = \frac{R_{bulk}}{N_T^W} N_\alpha \rho_\alpha \quad (3)$$

$$\beta = \frac{\omega_{RL}^2}{N_T^W} N_\beta S_\beta^2 \quad (4)$$

and a relation for γ analogous to eq 4. Here, N_T^W is the water/protein molar ratio (see above) and ω_{RL} is the rigid-lattice quadrupole coupling frequency: 8.70×10^5 rad/s for ^{2}H and 76.1×10^5 rad/s for ^{17}O (*44*, *45*). In eq 3, N_α is the number of water molecules in contact with the protein surface, and the rotational retardation factor ρ_α ($=\langle\tau_\alpha\rangle/\tau_{bulk} - 1$) is a measure of the average surface-induced retardation of the rotational motion of these water molecules, relative to bulk water.

In eq 4, N_β is the number of water molecules that are associated with the protein for a sufficiently long time (>1 ns) to give rise to an observable frequency dependence in R_1. The root-mean-square orientational order parameter of these long-lived water molecules is denoted S_β, and their correlation time, τ_β, is given by (*44*, *45*)

$$\frac{1}{\tau_\beta} = \frac{1}{\tau_R} + \frac{1}{\tau_W} \quad (5)$$

where τ_W is the mean residence time for the N_β water molecules and τ_R is the rotational correlation time of the protein. A similar relation holds for τ_γ. By convention, the γ dispersion occurs at a higher frequency than the β dispersion, meaning that $\tau_\gamma < \tau_\beta$. Typically, the β dispersion reflects internal water molecules for which $\tau_W \gg \tau_R$ so that $\tau_\beta = \tau_R$, whereas the γ dispersion is associated with more mobile internal water molecules, for which $\tau_\gamma < \tau_R$. For example, lipid binding proteins contain a large cluster of internal water molecules that exchange positions on a time scale of ~1 ns, and τ_γ may then be identified with this internal exchange time (*53*, *70*).

Analysis of ^{19}F MRD Data. The ^{19}F nuclei in TFE are relaxed by dipole−dipole couplings. In place of eq 1, we then have (*44*, *45*)

$$R_1(\omega_0) = R_{bulk} + 0.2J_{FF}(\omega_F) + 0.8J_{FF}(2\omega_F) + 0.1J_{FH}(\omega_H - \omega_F) + 0.3J_{FH}(\omega_F) + 0.6J_{FH}(\omega_H + \omega_F) \quad (6)$$

where ω_F and ω_H are the ^{19}F and ^{1}H (angular) resonance frequencies, respectively. The SDFs $J_{FF}(\omega)$ and $J_{FH}(\omega)$ are still given by eq 2, although a γ dispersion was not observed for ^{19}F, but eqs 3 and 4 are replaced by

$$\alpha = \alpha_{FF} + \alpha_{FH} = \frac{R_{bulk}}{N_T^{TFE}} N_\alpha \rho_\alpha \quad (7)$$

$$\beta_{FF} = 2 \times \frac{3}{2} \frac{\omega_{FF}^2}{N_T^{TFE}} N_\beta S_\beta^2 \quad (8a)$$

$$\beta_{FH} = 2 \frac{\omega_{FH}^2}{N_T^{TFE}} N_\beta S_\beta^2 \quad (8b)$$

where N_T^{TFE} is the TFE/protein molar ratio and N_α, ρ_α, N_β, and S_β now refer to TFE rather than to water. The factor of 2 in eq 8 appears because each ^{19}F nucleus is dipole-coupled to two other ^{19}F nuclei in the CF_3 group or to two protons in the adjacent CH_2 group. The factor of $^3/_2$ in eq 8a reflects cross relaxation within a homonuclear pair of dipole-coupled nuclei (*54*). The rigid-lattice dipole coupling frequencies ω_{FF} and ω_{FH} in eq 8 refer to bound TFE molecules that tumble with the protein and are averaged over the much faster internal rotation of the CF_3 group. Therefore

$$\omega_{FF} = \left(-\frac{1}{2}\right)\frac{\mu_0}{4\pi} \frac{\hbar\gamma_F^2}{r_{FF}^3} \quad (9a)$$

$$\omega_{FH} = \frac{\mu_0}{4\pi}\hbar\gamma_F\gamma_H \left\langle \frac{P_2(\cos\theta)}{r_{FH}^3} \right\rangle \quad (9b)$$

In both cases, the symmetry axis of the averaged dipole−dipole coupling tensor is along the internal rotation axis (the C−C bond). The factor of $-^1/_2$ in eq 9a arises because the F−F vectors are perpendicular to this axis. The angular brackets in eq 9b signify averaging over the internal rotation, which modulates the F−H separation r_{HF} as well as the angle θ between the F−H vector and the C−C bond. In writing eq 9b, we have neglected the small asymmetry of the motionally averaged F−H dipole−dipole coupling tensor. Using the molecular geometry determined (*55*) by X-ray diffraction on liquid TFE ($r_{FF} = 214.4$ pm, $r_{CF} = 136.0$ pm, $r_{CC} = 152.6$ pm, and $\theta_{FCC} = 103°$) along with the standard values for r_{CH} of 109 pm and for θ_{CCH} of 109° and assuming free rotation about the C−C bond, we obtain the following values: $\omega_{FF} = -3.39 \times 10^4$ rad/s and $\omega_{FH} = 2.39 \times 10^4$ rad/s. The fast internal rotation of the CF_3 group also gives a (negligibly small) contribution to the frequency-independent α term in eq 7.

Table 2: Results of Fits to ^{2}H, ^{17}O, and ^{19}F MRD Data[a]

no.[b]	T (°C)	TFE (vol%)	nucleus	τ_β (ns)	τ_γ (ns)	$N_\beta S_\beta^2$	$N_\gamma S_\gamma^2$	$N_\alpha \rho_\alpha$ ($\times 10^3$)	R_{bulk} (s^{-1})
1	4	0	^{2}H	16 (6)	4 (2)	8 (3)	14 (5)	6 (1)	3.84 (1)
1	4	0	^{17}O	17 (6)	3 (1)	2.2 (8)	9 (6)	3 (1)	285 (1)
2	4	16	^{2}H	34 (33)	6 (2)	7(2)	18 (3)	4.3 (6)	6.91 (3)
2	4	16	^{17}O	[34]	2.5 (5)	1.7(2)	17 (4)	1.2 (5)	517 (1)
3	4	30	^{2}H	23 (4)	2.6 (8)	10 (2)	32 (13)	0.2 (1.1)	8.70 (3)
3	4	30	^{17}O	–	1.6 (8)[c]	–	13 (25)[c]	0.8 (1.2)	641 (1)
4	27	0	^{2}H	6.3 (3)	–	7.2 (4)	–	2.4 (3)	1.93 (1)
4	27	0	^{17}O	7.3 (6)	–	2.6 (3)	–	2.4 (3)	142.9 (1)
5	27	16	^{2}H	24 (4)	2.6 (1.3)	3.2 (4)	6 (4)	1.2 (1.0)	2.88 (2)
5	27	16	^{17}O	[24]	1.9 (1.1)	0.5 (1)	7 (14)	0.4 (2.3)	211 (1)
6	27	29	^{2}H	40 (29)	5 (2)	2.2 (4)	4.2 (8)	0.5 (3)	3.35 (2)
6	27	29	^{17}O	[40]	–	0.14 (5)	–	0.6 (1)	239 (1)
7	27	7	^{19}F	7 (1)	–	4.5 (3)	–	0.15 (2)	0.161 (2)
8	27	21	^{19}F	4 (1)	–	6 (2)	–	0.35 (9)	0.184 (3)

[a] Parameter uncertainty (one standard deviation) in last digit given in parentheses. Brackets indicate that the parameter value was frozen during the fit. All fits were bi-Lorentzian, except when no values are given for the γ parameters. [b] Each number corresponds to a different sample; see Table 1. [c] This single-Lorentzian MRD profile was assigned to the γ dispersion.

The preceding discussion of ^{19}F relaxation invoked several approximations. First, we have assumed that the ^{19}F nuclei in TFE are relaxed entirely by the dipole−dipole mechanism, neglecting any contributions from the shielding anisotropy and spin-rotation mechanisms (*56*). The neglect of the shielding anisotropy contribution to R_1, which increases quadratically with the magnetic field (and ω_F), is justified by the observation that R_1 for the reference samples is constant up to the highest ^{19}F frequency that was used (94 MHz). (R_1 data obtained at 188 MHz indicate a small shielding anisotropy contribution and were therefore not included in the analysis.) A ^{19}F relaxation study (*57*) of neat TFE showed that the spin-rotation mechanism contributes significantly to R_1 at elevated temperatures (48 and 66 °C). The spin-rotation contribution may be negligible, considering that we work at lower temperatures and that the internal rotation of the CF_3 group should be slower in aqueous solution than in neat TFE. In any case, because the internal rotation occurs on a picosecond time scale, a spin-rotation contribution will only affect the α parameter. Another approximation is our neglect of dipole−dipole couplings between ^{19}F and protons in water and in the hydroxyl group of TFE. This simplification is justified by the longer distances (the F atoms of TFE are poor hydrogen bond acceptors) and the 50% H → D substitution in our solvent. Finally, we have ignored cross-correlation effects in the ^{19}F three-spin system of the CF_3 group. Theoretical analysis of the analogous CH_3 system (*58*) indicates that such effects are very small. Consistent with this, we observed monoexponential ^{19}F relaxation in all cases.

RESULTS

We have measured the longitudinal relaxation rate R_1 of the water ^{2}H and ^{17}O magnetizations and of the TFE ^{19}F magnetization as a function of the resonance frequency ν_0 at two temperatures (4 and 27 °C) for solutions of BLG in water and in mixed TFE/water solvents (7−30% TFE, v/v). At 27 °C, BLG is expected to be fully converted to the helical state at 30% TFE (*13*, *22*, *26*), while the intermediate state should predominate at 16% TFE (*26*). In addition, we have measured the frequency-independent R_1 for reference samples with the same solvent composition as in the protein solutions. This quantity, denoted R_{bulk}, is given in Table 2 for the samples that have been investigated.

The ^{17}O and ^{19}F MRD profiles $R_1(\nu_0)$ exclusively monitor the microdynamical behavior of water molecules and TFE molecules, respectively. A frequency dependence in R_1 below ca. 100 MHz can therefore be taken as unequivocal evidence for long-lived (>1 ns) association of water (^{17}O) or TFE (^{19}F) molecules with the protein. The ^{2}H magnetization derives mainly from water molecules, but also has contributions from labile hydrogens in BLG and TFE that exchange with water hydrogens on the relaxation time scale (*50*, *51*). The ^{2}H MRD profile can therefore provide the rotational correlation time τ_R of the protein even in the absence of long-lived water or TFE association.

In the simplest case, the MRD profile yields three parameters: α, β, and τ_β. The α parameter is the excess relaxation ($R_1 - R_{bulk}$) on the high-frequency plateau of the MRD profile, and it characterizes the dynamical perturbation of solvent molecules at the protein surface (*44*, *45*). This perturbation is expressed as the product of the number N_α of solvent molecules (water or TFE) in contact with the protein surface and the relative retardation ρ_α of their rotational motion (see Materials and Methods). The dispersion amplitude parameter β yields the product of the number N_β of solvent molecules in long-lived association with the protein and their mean-square orientational order parameter S_β^2 (see Materials and Methods). The correlation time τ_β is equal to or shorter than the rotational correlation time τ_R of the protein (see eq 5). In the case of BLG, the ^{2}H and ^{17}O MRD profiles exhibit a second dispersion step at higher frequencies. This introduces two additional parameters γ and τ_γ, analogous to β and τ_β, respectively.

Figures 1 and 2 show ^{2}H and ^{17}O MRD profiles measured at 4 °C on BLG solutions containing 0, 16, or 30% TFE. To highlight nontrivial cosolvent effects, we present the relaxation data in a normalized form. We have thus subtracted the bulk solvent relaxation rate R_{bulk}, which varies by a factor of 2.26 ± 0.01 between 0 and 30% TFE (Table 2). The finding that the relative increase in R_{bulk} on addition of TFE is the same for ^{2}H and ^{17}O indicates that the hydroxyl hydrogens of TFE, which account for 5% of the ^{2}H magnetization in the 30% TFE solvent, do not affect the observed ^{2}H relaxation rate significantly. While the protein

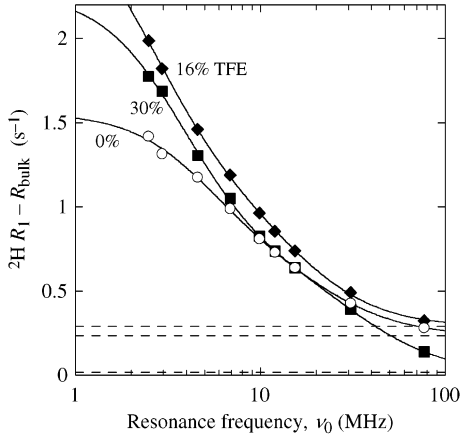

FIGURE 1: Water ^{2}H MRD profiles recorded at 4 °C for BLG solutions at pH 2.4 and the indicated TFE concentration. The dispersion curves resulted from fits according to eqs 1 and 2. Relaxation data are presented as the excess relaxation rate $R_1 - R_{bulk}$, scaled to the same water/BLG molar ratio ($N_T^W = 1.036 \times 10^5$) for all samples. The uncertainty in R_1 is comparable to the size of the data symbols. The scaled high-frequency plateau, α, is indicated by dashed lines, from top to bottom: 16, 0, and 30% TFE.

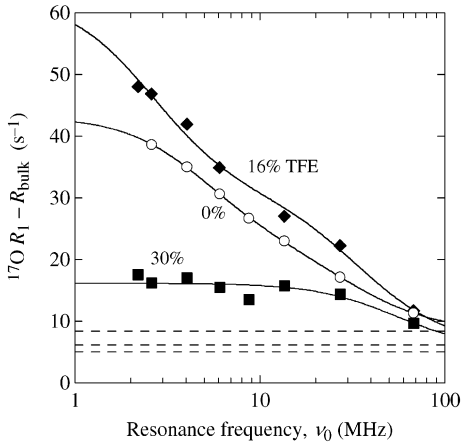

FIGURE 2: Water ^{17}O MRD profiles recorded at 4 °C for BLG solutions at pH 2.4 and the indicated TFE concentration. The dispersion curves resulted from fits according to eqs 1 and 2. Relaxation data are presented as the excess relaxation rate $R_1 - R_{bulk}$, scaled to the same water/BLG molar ratio ($N_T^W = 1.036 \times 10^5$) for all samples. The uncertainty in R_1 is approximately twice the size of the data symbols. The scaled high-frequency plateau, α, is indicated by dashed lines, from top to bottom: 0, 16, and 30% TFE.

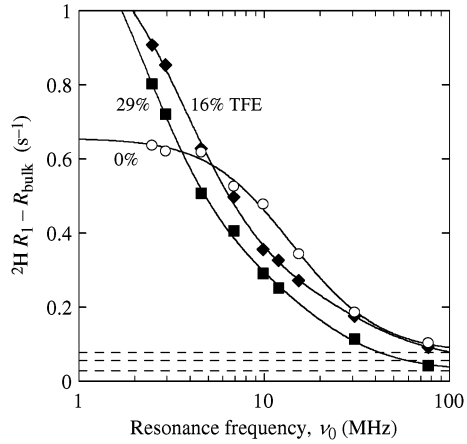

FIGURE 3: Water ^{2}H MRD profiles recorded at 27 °C for BLG solutions at pH 2.4 and the indicated TFE concentration. The dispersion curves resulted from fits according to eqs 1 and 2. Relaxation data are presented as the excess relaxation rate $R_1 - R_{bulk}$, scaled to the same water/BLG molar ratio ($N_T^W = 5.94 \times 10^4$) for all samples. The uncertainty in R_1 is comparable to the size of the data symbols. The scaled high-frequency plateau, α, is indicated by dashed lines, from top to bottom: 0, 16, and 29% TFE.

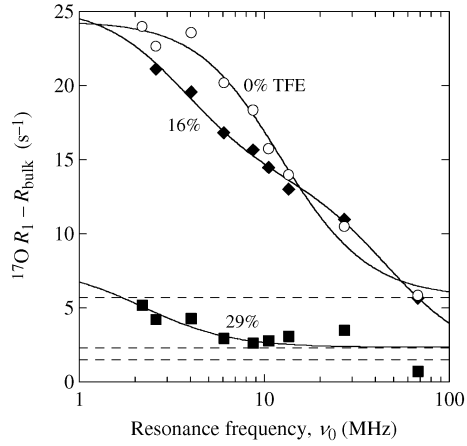

FIGURE 4: Water ^{17}O MRD profiles recorded at 27 °C for BLG solutions at pH 2.4 and the indicated TFE concentration. The dispersion curves resulted from fits according to eqs 1 and 2. Relaxation data are presented as the excess relaxation rate $R_1 - R_{bulk}$, scaled to the same water/BLG molar ratio ($N_T^W = 5.94 \times 10^4$) for all samples. The uncertainty in R_1 is approximately twice the size of the data symbols. The scaled high-frequency plateau, α, is indicated by dashed lines, from top to bottom: 0, 29, and 16% TFE.

concentration is similar in the three samples, the water/BLG ratio N_T^W varies substantially (Table 1). This trivial variation is carried over to the excess relaxation rate $R_1 - R_{bulk}$, which is inversely proportional to N_T^W (see eqs 1−4). We have therefore normalized the excess relaxation rate to the same N_T^W value for all three samples.

With one exception (see below), all MRD profiles recorded at 4 °C are bi-Lorentzian; i.e., both the β and γ terms in the SDF of eq 2 are statistically justified (see Materials and Methods). The parameter values derived from the fits are collected in Table 2. Because the β and γ dispersions overlap, the parameters cannot be determined with high accuracy. Furthermore, the incomplete sampling of the β dispersion in some cases results in a substantial uncertainty in the correlation time τ_β . An unconstrained bi-Lorentzian fit to the ^{17}O MRD data at 16% TFE leads to unphysical parameter values. We therefore constrained τ_β to the value determined from the corresponding ^{2}H profile. This procedure is justified by the expectation that τ_β reflects protein rotation in both cases. The ^{17}O data at 30% TFE do not exhibit any significant frequency dependence below 10 MHz, and the small dispersion seen at higher frequencies was assigned to the γ term.

The ^{2}H and ^{17}O MRD profiles measured at 27 °C are shown in Figures 3 and 4, and the parameter values resulting from the fits are given in Table 2. At this temperature, unconstrained bi-Lorentzian fits were possible in two cases only. In the absence of TFE, both ^{2}H and ^{17}O dispersions are described well by a single-Lorentzian SDF, but the value of the correlation time indicates that it represents two strongly overlapping dispersions (see Discussion). At the intermediate

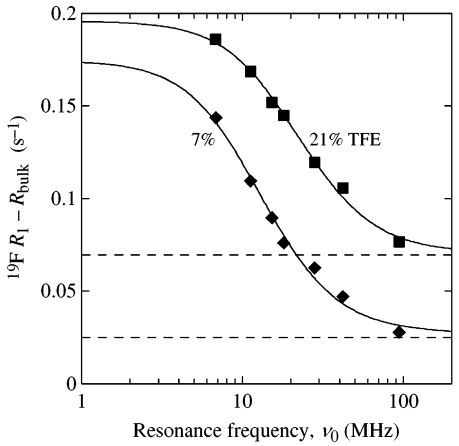

FIGURE 5: TFE ^{19}F MRD profiles recorded at 27 °C for BLG solutions at pH 2.4 and the indicated TFE concentration. The dispersion curves resulted from fits according to eqs 2 (without the γ term) and 6. Relaxation data are presented as the excess relaxation rate $R_1 - R_{bulk}$, scaled to the same TFE/BLG molar ratio ($N_T^{TFE} = 970$) for both samples. The uncertainty in R_1 is approximately twice the size of the data symbols. The scaled high-frequency plateau, α, is indicated by dashed lines.

TFE concentration, the ^{17}O correlation time τ_β was constrained to the ^{2}H value, as for the 4 °C data. At the highest TFE concentration (29%), the ^{17}O profile appears to be single-Lorentzian, but in contrast to the corresponding 4 °C profile, the dispersion must now be assigned to the β term.

^{19}F MRD profiles, which monitor TFE−protein interactions, were recorded at 27 °C in the presence of 7 and 21% TFE (see Figure 5 and Table 2). In presenting the ^{19}F data, we have subtracted R_{bulk} and normalized the resulting excess relaxation rate to the same value of the TFE/BLG ratio N_T^{TFE}. Both ^{19}F profiles are described well by a single-Lorentzian SDF. To simplify the interpretation, the fits are based on data from the frequency range where only dipole−dipole couplings (rather than shielding anisotropy) contribute significantly to ^{19}F relaxation (see Materials and Methods).

While the model parameters cannot always be determined with high accuracy, the MRD profiles in Figures 1−5 display a strong and nontrivial dependence on TFE concentration. We now turn to the quantitative analysis of this dependence and the implications for our understanding of the TFE-induced $\beta \rightarrow \alpha$ transition in BLG and the nature of the nonnative helical states.

DISCUSSION

Internal and External Hydration of Native BLG. We focus here on MRD data recorded at 4 °C, where the β and γ dispersions are separable. In the absence of TFE, the ^{2}H and ^{17}O profiles yield essentially the same correlation times: $\tau_\beta = 16-17 \pm 6$ ns and $\tau_\gamma = 3-4 \pm 2$ ns. The rotational correlation time of native BLG (1 mM) at pH 2.6 and 37 °C has been determined to be 7.3 ± 0.1 ns by ^{15}N relaxation (*32*). With τ_R proportional to η/T, this value translates into 19.6 ns at 4 °C and our solvent isotope composition. We can therefore identify τ_β with the rotational correlation time of BLG. The $N_\beta S_\beta^2(^{17}O)$ value of 2.2 ± 0.8 implies that native BLG contains at least two water molecules with a residence time τ_W of $\gg$20 ns at 4 °C. Such long residence times indicate buried hydration sites (*42*, *43*). An analysis of the 1.8 Å resolution crystal structure 1BEB (*30*) does indeed reveal two such water molecules, neither of which resides in the hydrophobic binding cavity.

Because $\tau_\gamma \ll \tau_R$, the shorter correlation time must reflect water exchange. The value of $N_\gamma S_\gamma^2(^{17}O)$ implies that BLG contains at least 9 ± 6 water molecules with a mean residence time of 3−4 ns at 4 °C. In the crystal structure, six water molecules are located in deep surface pockets and could have residence times in this range. None of these potentially long-lived water molecules are found in the large binding cavity, which appears to be empty in the crystal structure. More likely, this cavity contains positionally disordered water molecules that escape detection by X-ray diffraction but might contribute to the γ dispersion. With a contact volume of 530 Å^3 (calculated on the 1BEB structure with a probe radius of 1.2 Å), the binding cavity could accommodate 15−20 water molecules. As in the case of lipid-binding proteins (*53*, *70*), the γ dispersion may reflect intracavity site exchange within a moderately ordered internal water cluster (*59*).

The quantity $N_\alpha \rho_\alpha$ [$(3 \pm 1) \times 10^3$] is a global measure of the dynamic perturbation of water molecules in contact with the protein surface (*44*, *45*). The solvent-accessible surface area of native BLG is 85 nm^2 (*60*). If a water molecule occupies 0.15 nm^2, this yields an N_α of 570 and a ρ_α of 5.3 ± 1.8, which is within the typical range (4−5) for globular proteins (*42*, *43*).

Whereas the ^{17}O magnetization derives exclusively from water molecules, the ^{2}H magnetization also has contributions from labile hydrogens exchanging rapidly with water hydrogens. The ^{2}H MRD profile thus reflects water molecules as well as labile hydrogens in the hydroxyl group of TFE and at 48 sites in the protein (28 COOH groups, 19 OH groups, and one SH group). At pH 2.4, the residence times of these labile hydrogens are expected to be in the range of 0.1−100 μs. Using intrinsic relaxation rates and hydrogen exchange rate constants determined for bovine pancreatic trypsin inhibitor, but converted to our temperature and H/D isotope composition (*61*−*63*), we estimate that labile hydrogens in BLG contribute 4.5 units to $N_\beta S_\beta^2$ at both 4 and 27 °C. This rough estimate is consistent with the observed difference between $N_\beta S_\beta^2(^2H)$ and $N_\beta S_\beta^2(^{17}O)$ (Table 2). Finally, the 2-fold larger value of $N_\alpha \rho_\alpha$ for ^{2}H, compared to that for ^{17}O, can be attributed to fast internal motions of side chains bearing labile hydrogens (*63*).

At 27 °C, the strong overlap of the β and γ dispersions prevents a bi-Lorentzian fit. As expected, the single apparent correlation time (6.3 ± 0.3 ns for ^{2}H and 7.3 ± 0.6 ns for ^{17}O) is significantly shorter than the predicted rotational correlation time of BLG at this temperature [$\tau_R = 9.6$ ns (Table 1)]. The $N_\beta S_\beta^2$ and $N_\alpha \rho_\alpha$ values are in the expected range, but a quantitative analysis is precluded by the β/γ overlap.

Hydration and Structure of the Nonnative States of BLG Induced by TFE. Each of the five model parameters that describe the water ^{2}H and ^{17}O MRD profiles can provide information about the nonnative BLG states induced by TFE. To the extent that τ_β reflects protein tumbling, it gives a measure of the hydrodynamic volume of the protein. For reference purposes, we give in Table 1 the rotational correlation time predicted for the *native* protein in the mixed solvents. These τ_R estimates are based on the theoretically

predicted η/T scaling and known viscosities for TFE/H_2O mixtures (*64*, *65*). The H/D isotope effect was taken to be the same as in the absence of TFE. The parameter $N_\beta S_\beta^2$-(^{17}O) is a measure of the number of long-lived hydration sites and thus reports on the structural integrity of the protein. The parameters $N_\gamma S_\gamma^2$ and τ_γ presumably reflect the status of the large binding cavity, while $N_\alpha \rho_\alpha$ reports on global solvent exposure and preferential solvation. This last parameter will be discussed in connection with the ^{19}F MRD data.

We consider first the state of BLG at the intermediate TFE concentration (16%). Here the MRD results show clear differences between the two temperatures. At 4 °C, the finding that $N_\beta S_\beta^2$ is not significantly affected by 16% TFE for either ^2H or ^{17}O indicates that BLG retains a compact native-like structure at 16% TFE. The increase in τ_β between 0 and 16% TFE can be largely explained by the enhanced solvent viscosity (see Tables 1 and 2) and is therefore consistent with a native-like structure at 16% TFE. At room temperature, 16% TFE is close to the midpoint of the N ↔ H transition (*13*, *22*, *26*), where the I state is highly populated (*26*). However, the $^1H-^{15}N$ HSQC NMR spectrum of BLG in 15% TFE was reported to be close to that of native BLG at temperatures below 15 °C (*23*). This observation is in full accord with our MRD results at 4 °C.

At 27 °C and 16% TFE, the correlation time τ_β of 24 ± 4 ns significantly exceeds the rotational correlation time τ_R of 14.6 ns predicted for the native protein at this solvent viscosity. This implies that the hydrodynamic volume of the protein has increased by 65 ± 30%, consistent with the prevalent view of the TFE-induced helical states as a relatively open assembly of weakly interacting helical segments (*13*). A substantial structural change is also signaled by the 4-fold reduction in $N_\beta S_\beta^2$(^{17}O), which indicates that the long-lived hydration sites are largely disrupted. A parallel reduction in $N_\beta S_\beta^2$(^2H) is observed, and the residual value can largely be attributed to labile BLG hydrogens (possibly with a reduced order parameter). Our results at 27 °C and 16% TFE pertain to the I state, judging from deconvoluted CD spectra (*26*).

At our highest TFE concentration (29 or 30%), BLG should be fully converted to the H state at 27 °C (*13*, *22*, *26*). Consistent with this expectation, τ_β is approximately twice as long (but with a large uncertainty) as the τ_R predicted for the native protein, implying a correspondingly large expansion of the protein. A progressive expansion of BLG upon going from 0 to 16 to 29% is also indicated by the continued decrease of the $N_\beta S_\beta^2$ parameter for both nuclei. The small value of $N_\beta S_\beta^2$(^{17}O) (0.14 ± 0.05) presumably reflects several weakly ordered water molecules that penetrate the open H state, while the further drop in $N_\beta S_\beta^2$(^2H) may be caused by increased flexibility of side chains carrying labile hydrogens.

We see a qualitative difference between the MRD results at the two temperatures also at the highest TFE concentration. This difference is most pronounced for the ^{17}O profile, which lacks a β dispersion at 4 °C. This demonstrates that the (two or more) long-lived hydration sites present in the native protein no longer exist. If the (small) β dispersion seen at 27 °C and 29% TFE is produced by weakly ordered water molecules that penetrate the expanded protein, then we must conclude that such water penetration does not occur at 4 °C. This could be because the protein is more compact or because only TFE molecules penetrate the protein at the lower temperature. The ^2H correlation time (τ_β = 23 ± 4 ns) is surprisingly short even for a moderately expanded protein. In fact, it is only half of the τ_R predicted for the native protein. Two phenomena may contribute to this anomaly. First, if the open helical structure is much less rigid than the native protein, several correlation times are needed to model the rotation and the slowest of these rotational modes might fall outside our frequency window. Second, the labile hydroxyl hydrogens on TFE molecules in long-lived association with the protein contribute to the ^2H profile. If this contribution is significant, then the observed τ_β can be reduced by TFE exchange, as is the case for the ^{19}F profiles (see below).

TFE−Protein Interactions. The most clear-cut results of this study are the ^{19}F MRD profiles in Figure 5. These dispersions conclusively demonstrate long-lived binding of TFE to the protein. The correlation time τ_β of the single-Lorentzian dispersion is 7 ± 1 ns at 7% TFE and 4 ± 1 ns at 21% TFE, both at 27 °C. These values are shorter than the rotational correlation time predicted for the *native* protein at these TFE concentrations (Table 1). More importantly, they are severalfold shorter than the τ_β values derived from the ^2H profiles at 27 °C in the presence of TFE (Table 2). The ^{19}F MRD data therefore show that the residence time of TFE molecules bound to BLG is in the range of 5−10 ns at 27 °C (see eq 5). The values obtained for the parameter $N_\beta S_\beta^2$ imply that BLG contains *at least* five such long-lived TFE molecules. Since the mean-square molecular order parameter S_β^2 may be well below its rigid binding limit of 1, the number N_β of long-lived TFE molecules may exceed the lower bound of 5 by an order of magnitude.

According to CD and high-resolution NMR studies (*13*, *22*, *23*, *26*), BLG retains its native structure at 7% TFE, whereas at 21% TFE, the I and H states are present at roughly equal populations without any coexisting native protein. The ^{19}F MRD data thus lead us to the intriguing conclusion that $N_\beta S_\beta^2$ is nearly the same in the native and TFE-induced states. However, the TFE sites are not necessarily the same in the different protein states. In fact, this is highly improbable, judging from the strong variation of the ^2H and ^{17}O profiles with TFE concentration. A more likely scenario is that the native state has a relatively small number of long-lived binding sites with large S_β^2 values, whereas the I and H states are penetrated by a considerably larger number of less ordered TFE molecules.

As for water, TFE residence times in the nanosecond range cannot be rationalized solely in terms of favorable hydrogen bonds and other noncovalent interactions. These interactions are also present in the bulk solvent, where molecular motions take place on a picosecond time scale. Instead, long residence times result from trapping of solvent molecules within the protein structure. In the native protein at 7% TFE, the most likely sites for long-lived TFE molecules are the deep surface pockets seen in the crystal structure (*30*). If the water molecules that occupy these pockets in the absence of TFE have residence times on the order of 100 ps, their preferential occupation by TFE molecules should be accompanied by a reduction of $N_\alpha \rho_\alpha$(^{17}O). Although ^{17}O data at 7% TFE are not available, such a reduction is seen at 16% TFE (Table 2).

A variation of $N_\alpha\rho_\alpha$ with TFE concentration can be produced in several ways. If the protein expands, the solvent-accessible surface area increases. If the solvent is water, we expect N_α to increase roughly in proportion to the accessible area. In a mixed solvent, however, preferential solvation complicates the picture. In addition, the rotational retardation factor ρ_α may change depending on the nature of the newly exposed surface and the composition of the solvation layer. In the absence of independent information, it is difficult to disentangle these contributing factors. Nevertheless, some semiquantitative inferences can be made.

At 30% TFE, $N_\alpha\rho_\alpha(^{17}O)$ is reduced from its value for pure water by a factor 4 (at both temperatures) even though the expanded state of BLG should have a larger solvent-accessible area than the native state. The main cause of this reduction is presumably the replacement of water with TFE at the protein surface. If the protein surface were completely covered by TFE, then $N_\alpha\rho_\alpha(^{17}O)$ would pertain to the water molecules in contact with this TFE layer. From the observed variation of $R_{bulk}(^{17}O)$ with TFE concentration, we obtain an $N_\alpha\rho_\alpha$ value of 12. Taking the water coordination number N_α of TFE to be 20, we then obtain a retardation factor ρ_α of 0.6. For a TFE-covered protein, we thus estimate that $N_\alpha\rho_\alpha(^{17}O) \approx 600 \times 0.6 = 360$. The slightly higher observed value, 600 ± 100 (Table 2), is consistent with some residual direct water−protein contact (with a larger retardation factor).

If the large reduction of $N_\alpha\rho_\alpha(^{17}O)$ is due to replacement of water with TFE at the protein surface, it should be accompanied by an increase in $N_\alpha\rho_\alpha(^{19}F)$. This is indeed observed; $N_\alpha\rho_\alpha(^{19}F)$ increases from 150 ± 20 at 7% TFE to 350 ± 90 at 21% TFE. Because the retardation factor ρ_α is not known for TFE, we cannot deduce the number N_α of TFE molecules in contact with the protein surface. TFE is known to be a poor hydrogen bond acceptor (*66*) and to interact only weakly with peptides (*39*), primarily via hydrogen bonds donated by the TFE hydroxyl group to the carbonyl oxygen of peptide groups (*40*). In simulations, TFE and water have comparable residence times at the peptide surface despite the larger size of TFE (*40*). For these reasons, we expect ρ_α to be smaller, perhaps even <1, for TFE than for water. Given that the ratio of the molar volumes of water and TFE is 4 (*50*), a crude estimate of the number of TFE molecules needed to cover the surface of native BLG is $570/4^{2/3}$ ($\approx$225). In the expanded state, this number would be larger.

Taken together, these crude estimates are consistent with several hundred moderately perturbed ($\rho_\alpha \approx 1$) TFE molecules at the protein surface. If water and TFE were uniformly distributed throughout the solvent, then only approximately 30 TFE molecules would make contact with 85 nm^2 of protein surface (as in the native protein) at 21% TFE (where there are 15 water molecules for every TFE molecule). To account for an $N_\alpha\rho_\alpha(^{19}F)$ of 350, we would then need a retardation factor of $\sim$10, which is clearly unrealistic. In conclusion, then, the ^{19}F MRD data indicate that BLG has a strong preference for solvation by TFE. This is in accord with the 2−3-fold TFE enrichment in the surface layer of peptides in 30% TFE seen in several simulations (*37*−*39*).

CONCLUSIONS

The ^2H, ^{17}O, and ^{19}F MRD data presented here offer a new perspective on the TFE-induced $\beta \rightarrow \alpha$ transition of β-lactoglobulin. Unlike the traditional techniques used in this field, the MRD method focuses directly on the solvent, providing quantitative information about preferential solvation and solvent penetration as well as about the overall size and structural integrity of the protein.

At 27 °C, the consecutive structural transformations of N(0% TFE) → I(16% TFE) and of I(16% TFE) → H(29% TFE) were found to be accompanied by a progressive expansion of the protein and loss of specific long-lived hydration sites. The observation of ^{17}O and ^{19}F dispersions when the protein is in the open helical (H) state conclusively demonstrates long-lived association of water (>40 ns) and TFE (5−10 ns) with the expanded protein. These long residence times indicate that solvent molecules penetrate the protein matrix. The number of such long-lived internal TFE molecules is $\sim 5/S_\beta^2$, with the mean-square molecular order parameter S_β^2 in the range of 0−1. When the protein transforms from the native to the open helical state, the surface hydration parameter decreases by a factor 4, while the corresponding TFE parameter increases by a factor of 2 between 7 and 21% TFE. The MRD data are consistent with a strong accumulation of TFE at the surface as well as in the interior of the protein. Surprisingly, the ^{19}F MRD data also demonstrate long-lived binding of several TFE molecules in the native protein, presumably by displacement of water molecules in deep surface pockets.

At 4 °C, BLG is much less affected by TFE. The protein remains in the native state in the presence of 16% TFE, but adopts a nonnative structure at 30% TFE. This nonnative structure is not penetrated by long-lived water molecules, but presumably contains internal TFE molecules. In general, protein denaturation is driven by the very large conformational entropy of the unfolded state, which compensates for the loss of favorable interactions in the compact native state. The N → H transition may be rationalized in the same terms: the gain in conformational entropy is now smaller since only side chains are involved, but the loss of stabilizing interactions is also smaller because a TFE-rich solvent mixture occupies the interstitial space in the expanded protein. Presumably, internal water molecules satisfy hydrogen bond requirements, while the polarizable fluorine atoms of internal TFE molecules engage in favorable dispersion interactions with nonpolar side chains. For peptides, the accumulation of TFE in the contacting solvent layer is thought to be crucial for structural stabilization. To accomplish the same thing in a protein, TFE must not only accumulate at the protein surface but must also penetrate the protein to a larger extent than water does. This view is supported by the MRD data presented here.

The description of the open helical state as an expanded structure with a high content of regular (albeit nonnative) secondary structure but with flexible side chains comes close to the conventional view of the so-called molten globule state (*67*). As seen from the solvent, however, these nonnative states are distinct: whereas the helical state is permeated by solvent, the molten globule has native-like solvation (*47*). When present as kinetic folding intermediates, the open

helical state should therefore occur earlier on the folding pathway than the molten globule state.

REFERENCES

1. Goodman, M., Listowsky, I., and Masuda, Y. F. B. (1963) *Biopolymers 1*, 33−42.
2. Jasanoff, A., and Fersht, A. R. (1994) *Biochemistry 33*, 2129−2135.
3. Hamada, D., Kuroda, Y., Tanaka, T., and Goto, Y. (1995) *J. Mol. Biol. 254*, 737−746.
4. Rajan, R., and Balaram, P. (1996) *Int. J. Pept. Protein Res. 48*, 328−336.
5. Cammers-Goodwin, A., Allen, T. J., Oslick, S. L., McClure, K. F., Lee, J. H., and Kemps, D. S. (1996) *J. Am. Chem. Soc. 118*, 3082−3090.
6. Luo, P., and Baldwin, R. L. (1997) *Biochemistry 36*, 8413−8421.
7. Myers, J. K., Pace, C. N., and Scholtz, J. M. (1998) *Protein Sci. 7*, 383−388.
8. Hirota, N., Mizuno, K., and Goto, Y. (1998) *J. Mol. Biol. 275*, 365−378.
9. Kentsis, A., and Sosnick, T. R. (1998) *Biochemistry 37*, 14613−14622.
10. Walgers, R., Lee, T. C., and Cammers-Goodwin, A. (1998) *J. Am. Chem. Soc. 120*, 5073−5079.
11. Luo, P., and Baldwin, R. L. (1999) *Proc. Natl. Acad. Sci. U.S.A. 96*, 4930−4935.
12. Reiersen, H., and Rees, A. R. (2000) *Protein Eng. 13*, 739−743.
13. Shiraki, K., Nishikawa, K., and Goto, Y. (1995) *J. Mol. Biol. 245*, 180−194.
14. Buck, M. (1998) *Q. Rev. Biophys. 31*, 297−355.
15. Konno, T. (1998) *Protein Sci. 7*, 975−982.
16. Gast, K., Zirwer, D., Müller-Frohne, M., and Damaschun, G. (1999) *Protein Sci. 8*, 625−634.
17. Thomas, P. D., and Dill, K. A. (1993) *Protein Sci. 2*, 2050−2065.
18. Tanford, C., De, P. K., and Taggart, V. G. (1960) *J. Am. Chem. Soc. 82*, 6028−6034.
19. Dufour, E., and Haertle, T. (1990) *Protein Eng. 4*, 185−190.
20. Hirota, N., Mizuno, K., and Goto, Y. (1997) *Protein Sci. 6*, 416−421.
21. Uversky, V. N., Narizhneva, N. V., Kirschstein, S. O., Winter, S., and Lober, G. (1997) *Folding Des. 2*, 163−172.
22. Hamada, D., and Goto, Y. (1997) *J. Mol. Biol. 269*, 479−487.
23. Kuwata, K., Hoshino, M., Era, S., Batt, C. A., and Goto, Y. (1998) *J. Mol. Biol. 283*, 731−739.
24. Hirota-Nakaoka, N., and Goto, Y. (1999) *Bioorg. Med. Chem. 7*, 67−73.
25. Hong, D.-P., Hoshino, M., Kuboi, R., and Goto, Y. (1999) *J. Am. Chem. Soc. 121*, 8427−8433.
26. Mendieta, J., Folqué, H., and Tauler, R. (1999) *Biophys. J. 76*, 451−457.
27. Ragona, L., Confalonieri, L., Zetta, L., De Kruif, K. G., Mammi, S., Peggion, E., Longhi, R., and Molinari, H. (1999) *Biopolymers 49*, 441−450.
28. Kauffmann, E., Darnton, N. C., Austin, R. H., Batt, C., and Gerwert, K. (2001) *Proc. Natl. Acad. Sci. U.S.A. 98*, 6646−6649.
29. Gast, K., Siemer, A., Zirwer, D., and Damaschun, G. (2001) *Eur. Biophys. J. 30*, 273−283.
30. Brownlow, S., Morais Cabral, J. H., Cooper, R., Flower, D. R., Yewdall, S. J., Polikarpov, I., North, A. C. T., and Sawyer, L. (1997) *Structure 5*, 481−595.
31. Sawyer, L., and Kontopidis, G. (2000) *Biochim. Biophys. Acta 1482*, 136−148.
32. Uhrínová, S., Smith, M. H., Jameson, G. B., Uhrín, D., Sawyer, L., and Barlow, P. N. (2000) *Biochemistry 39*, 3565−3574.
33. Kontopidis, G., Holt, C., and Sawyer, L. (2002) *J. Mol. Biol. 318*, 1043−1055.
34. Sakurai, K., and Goto, Y. (2001) *Protein Sci. 10*, 2325−2335.
35. Kuroda, Y., Hamada, D., Tanaka, T., and Goto, Y. (1996) *Folding Des. 1*, 255−263.
36. Díaz, M. D., and Berger, S. (2001) *Magn. Reson. Chem. 39*, 369−373.
37. Fioroni, M., Díaz, M. D., Burger, K., and Berger, S. (2002) *J. Am. Chem. Soc. 124*, 7737−7744.
38. Díaz, M. D., Fioroni, M., Burger, K., and Berger, S. (2002) *Chem. Eur. J. 8*, 1663−1669.
39. Roccatano, D., Colombo, G., Fioroni, M., and Mark, A. E. (2002) *Proc. Natl. Acad. Sci. U.S.A. 99*, 12179−12184.
40. Iovino, M., Falconi, M., Marcellini, A., and Desideri, A. (2001) *J. Pept. Res. 58*, 45−55.
41. Martinez, D., and Gerig, J. T. (2001) *J. Magn. Reson. 152*, 269−275.
42. Denisov, V. P., and Halle, B. (1996) Protein hydration dynamics in aqueous solution, *Faraday Discuss. 103*, 227−244.
43. Halle, B. (1998) in *Hydration Processes in Biology* (Bellisent-Funel, M.-C., Ed.) pp 233−249, IOS Press, Dordrecht, The Netherlands.
44. Halle, B., Denisov, V. P., and Venu, K. (1999) in *Biological Magnetic Resonance* (Krishna, N. R., and Berliner, L. J., Eds.) pp 419−484, Kluwer/Plenum, New York.
45. Halle, B., and Denisov, V. P. (2001) *Methods Enzymol. 338*, 178−201.
46. Denisov, V. P., and Halle, B. (1998) *Biochemistry 37*, 9595−9604.
47. Denisov, V. P., Jonsson, B.-H., and Halle, B. (1999) *Nat. Struct. Biol. 6*, 253−260.
48. Jóhannesson, H., Denisov, V. P., and Halle, B. (1997) *Protein Sci. 6*, 1756−1763.
49. Privalov, A. F., Lips, O., and Fujara, F. (2002) *J. Phys.: Condens. Matter 14*, 4515−4525.
50. Gente, G., and La Mesa, C. (2000) *J. Solution Chem. 29*, 1159−1172.
51. Press, W. H., Flannery, B. P., Teukolsky, S. A., and Vetterling, W. T. (1992) *Numerical recipes in C. The art of scientific computing*, 2nd ed., Cambridge University Press, Cambridge, U.K.
52. Halle, B., Jóhannesson, H., and Venu, K. (1998) *J. Magn. Reson. 135*, 1−13.
53. Wiesner, S., Kurian, E., Prendergast, F. G., and Halle, B. (1999) *J. Mol. Biol. 286*, 233−246.
54. Abragam, A. (1961) *The Principles of Nuclear Magnetism*, Clarendon Press, Oxford, U.K.
55. Radnai, T., Ishigoro, S., and Ohtaki, H. (1989) *J. Solution Chem. 18*, 771−784.
56. Brey, W. S., and Brey, M. L. (1996) in *Encyclopedia of NMR* (Grant, D. M., and Harris, R. K., Eds.) pp 2063−2071, Wiley, Chichester, U.K.
57. Lambert, J. B., and Simpson, S. V. (1985) *Magn. Reson. Chem. 23*, 61−66.
58. Lee, T.-S., and Hwang, L.-P. (1990) *J. Magn. Reson. 89*, 51−59.
59. Bakowies, D., and van Gunsteren, W. F. (2002) *J. Mol. Biol. 315*, 713−736.
60. Oliveira, K. M., Valente-Mesquita, V. L., Botelho, M. M., Sawyer, L., Ferreira, S. T., and Polikarpov, I. (2001) *Eur. J. Biochem. 268*, 477−483.
61. Wüthrich, K., and Wagner, G. (1979) *J. Mol. Biol. 130*, 1−18.
62. Liepinsh, E., Otting, G., and Wüthrich, K. (1992) *J. Biomol. NMR 2*, 447−465.
63. Denisov, V. P., and Halle, B. (1995) *J. Mol. Biol. 245*, 698−709.
64. Kaiser, B., Laesecke, A., and Schmeck, M. (1989) *Int. J. Thermophys. 10*, 713−726.
65. Olivé, F., Chaudhari, S. K., Patil, K. R., and Coronas, A. (1996) *Can. J. Chem. Eng. 74*, 163−169.
66. Llinas, M., and Klein, M. P. (1975) *J. Am. Chem. Soc. 97*, 4731−4737.
67. Arai, M., and Kuwajima, K. (2000) *Adv. Protein Chem. 53*, 209−282.
68. Modig, K., Kurian, E., Prendergast, F. G., and Halle, B. (2003) *Protein Sci. 12* (12) (in press).
69. Gottschalk, M., Nilsson, H., Roos, H., and Halle, B. (2003) *Protein Sci. 12*, 2404−2411.
70. Modig, K., Rademacher, M., Lücke, C., and Halle, B. (2003) *J. Mol. Biol. 332*, 965−977.

BI035330L